Technische Universiteit Delft

Communications on Hydraulic and Geotechnical Engineering
2004-05

ISSN 0169-6548

The B009 data in the backward facing step experiment

——————— Report on the Data Analysis and evaluation———————

Nguyen Thanh Hoan*

November 15, 2004

*PhD Student, Section of Hydraulic Engineering, Faculty of Civil Engineering and Geosciences, Delft University of Technology, P.O. Box 5048, 2600 GA DELFT, The Netherlands. Tel. + 31 15 27 84736; Fax: +31 15 27 89453Email: hoan@dongchay.com

Contents

Table of contents **i**

Abstract **iii**

1 Problem description **1**
- 1.1 General introduction . . . 1
- 1.2 Work definition . . . 2
- 1.3 Objective . . . 2
- 1.4 Outline . . . 2

2 Physical concepts of stability **3**
- 2.1 Quasi-steady drag and lift forces . . . 3
- 2.2 Turbulence wall pressures (TWPs) . . . 6
- 2.3 Force-generating mechanisms . . . 6

3 Experimental set-up **8**
- 3.1 Introduction . . . 8
- 3.2 The target stone . . . 9
- 3.3 Flow parameters . . . 9
- 3.4 Equipment . . . 11

4 Data processing **12**
- 4.1 Introduction . . . 12
- 4.2 Visualized classification of events . . . 14
- 4.3 Inspection of vector plots . . . 14
- 4.4 Splicing . . . 15

5 Experiment Results **16**
- 5.1 Classification . . . 16
- 5.2 Conditional averages . . . 19
  - 5.2.1 Small-scale conditionally averaged flow structures . . . 20
  - 5.2.2 Large-scale spliced conditionally flow structure . . . 23
- 5.3 Instantaneous flow structure . . . 25
  - 5.3.1 Small-scale instantaneous flow structure . . . 25

5.3.2 Large-scale spliced flow structure 27

6 Conclusions and recommendations 30

6.1 Discussion 30

6.2 Conclusions 31

List of Symbols 33

List of Figures 35

References 36

Abstract

This report evaluates the B009 data of the back-ward facing step experiment which was one of a series of the experiments that were designed and conducted by Hofland and Booij (2004) and De Ruijter (2004). In this experiment, the flow field and the pressure field were measured (by PIV and pressure sensors) during the displacement of a single stone from a granular bed. This measurement shows similarities to the results from previous experiments. At the time the stone started to move, two flow structures were found to be responsible for the entrainment: a large-scale sweep ($u' > 0$ and $v' < 0$), causing increased quasi-steady forces, and an embedded small-scale structure with vertical velocity fluctuations, $\sigma(v')$, causing turbulence wall pressure fluctuation (TWP). In the four entrainments, these structures were present simultaneously in the instantaneous flow fields.

Chapter 1

Problem description

1.1 General introduction

In the equilibrium wall flow the forces on a bed particle scale with the shear stress, so for this flow the shear stress can be used as an indicator for entrainment and transport without knowing the exact force-generating mechanisms (Hofland, 2002). But in a non-equilibrium flow the situation is different. In such a flow, the fluctuating forces will play an important role in dislodging the stones, but they have hardly been studied.

Booij and Hofland (2004) distinguish two force-generating mechanisms that may be responsible for the entrainment of stones: quasi-steady force fluctuations (QSF), caused by large-scale motion ($u' > 0$, and usually $v' < 0$); and small-scale turbulence wall pressure fluctuations (TWP), caused by small-scale wall-normal fluctuations (v') and vortices. In these two mechanisms, the latter was newly proposed by Hofland.

In order to get a better understanding into both mechanisms (flow structures) of stone entrainment, Hofland develops the indicators for both mechanisms and did several experiments in which some flow configurations were made with a range of relative turbulence intensities and with a different character of the turbulent vortices: a uniform flow, a smooth bed to rough bed transition, a jet flow and a backward-facing step (BFS) flow. In these experiments, a La Vision PIV system was used to measure the data.

From the experiments, some important concepts on stability of stones have been proposed. However, not all the measurements have been evaluated due to the time and work. It is not easy to do such experiments with PIV technique so evaluating these data is really needed. In the probation of six months of my PhD study at Section of Hydraulics Engineering (TUDelft), I was assigned to evaluate these data. The work was supposed to be done in two months, starting in early September 2004.

1.2 Work definition

In the BFS experiments, two sets of data (B006 and B009) were obtained. Only the test B006 has been evaluated which gives some understanding on the mechanisms responsible for the entrainment of the stones. The test B009 which has not been evaluated will be dealt with in this report. In this report, comparison between the flow structures in the B009 and the flow structures in other flow configurations will also be made.

1.3 Objective

The objective is to investigate the structures responsible for and the mechanisms of the entrainment by the instantaneous and conditionally averaged flow field over the entrainment events in the experiment.

1.4 Outline

This report is structured as follows. The second Chapter examines theoretically the possible forces acting on a grain on bed under flow. The mechanisms that may be responsible for the entrainment of stones are also discussed. In Chapter 3 the experimental set-up is described. The following Chapter describes the data processing. Some techniques used to investigate the data are presented and discussed. Chapter 5 presents the results of the experiment. Comparison with the results from Hofland and Booij (2004) and De Ruijter (2004) is also made. Finally, in Chapter 6 some discussion and conclusions are presented.

Chapter 2

Physical concepts of stability

To understand the stability of loose grains (rock and gravel), it is necessary to know which forces make the stone move (Schiereck, 2001). The forces acting on a single grain can generally be divided into two types: ones that try to move the grain: the drag force (F_D), the lift force (F_L) and turbulence forces and ones which act to keep the grain in its place, the gravity force (=submerged weight = $(\rho_S - \rho)gV$, with V is the volume of the grain, ρ_S is the density of grain material, and ρ is the density of water), the contact forces. In the coarse bed material, there is no cohesive force. If the stone is placed in an accelerated flow, an extra added mass force is also present and act as an active force. In this chapter we will focus much on the drag, lift forces and turbulence forces. The mechanisms that may be responsible for the entrainment of stones are also discussed.

2.1 Quasi-steady drag and lift forces

If a grain is exposed into fluid flow, a frictional force F_1 is presented on the rough surface of the grain. This surface friction is the main force acting on the grain if the grain Reynolds number ($U * d/\nu$) less than 3.5. If the grain Reynolds number is larger than 3.5, however, separation of streamline in the form of a small wake occurs behind the top of the particles and vortexes form there. This causes a pressure difference between the font and the back surface of the particle, forming the resistance F_2. The resultant of F_1 and F_2 is called drag force (F_D) (Chien & Wan, 1998). When the grain Reynolds number is high, let's say, larger than 500, the frictional force F_1 can be negligible.

The velocity at the top is higher than the velocity at the bottom of the grain, causing a lift force (F_L). This lift force can be considered to act through the center of the grain.

Both drag force and lift force are the results of the pressure differences between the font and the back, the top and the bottom of the grain surface, which are the result of the difference of velocities. According to the Bernoulli law, these forces are

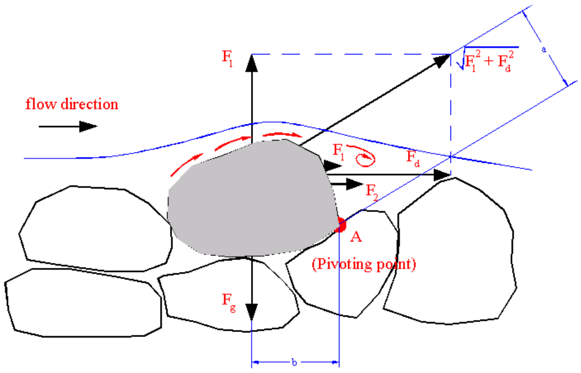

Figure 2.1: Forces acting on particles resting on the bed surface

proportional to the velocities in the vicinity of the grain. The drag force and the lift force can be expressed in general form as follows:

$$F_D = \frac{1}{2} C_D A_D \rho u|u| \tag{2.1}$$

$$F_L = \frac{1}{2} C_L A_L \rho u|u| \tag{2.2}$$

in which C_D and C_L are the drag and lift coefficients, respectively, and u is the velocity near the grain. A_D and A_L are the exposed surface areas. In general, A_D and A_L are proportional to the squared value of the nominal diameter d_n.

Much of research has been done on the drag and lift coefficients. The drag and lift coefficients depend on the flow pattern around the bed particle and the method of estimating u. The difference in definition of u in the vicinity of the grain causes the difference in the coefficient values. The common velocities used to determine drag and lift coefficients are $\bar{u}$ at $0.15d$ above the top of the grain, $\bar{u}$ measured at the height of the center of the grain, and shear velocity u_*. The coefficients become fairly constant for high grain Reynolds numbers, but most authors still find a small dependency of C_D on the grain Reynolds numbers (Hofland, 2002).

It can be seen from the previous research that the drag and lift coefficients are rather constant if $u_{0.15}$ is used as the reference velocity in Equation 2.1 and Equation 2.2. For this reference velocity, drag and lift coefficients are supposed to be constant and only depend on the shape of the grain, not on the flow conditions.

The averaged velocity near the stone is commonly used to determine the drag and lift forces. However, the velocity is not constant and the fluctuations of the velocities near the stone cause the forces to fluctuate as well. For this reason we refer to them as quasi-steady forces (QSF). We use this term in order to distinguish between these forces and another cause of the entrainment, the turbulent wall pressures (TWP) that are described later on (after Hofland & Booij, 2004 and De Ruijter, 2004). Generally, the fluctuating parts of velocity, u', is much less than the averaged value of velocity so $(u')^2 \ll (\bar{u})^2$ and the fluctuating parts of the drag and lift forces can be negligible. However, the velocity used in Equation 2.1 and Equation 2.2 is the velocity in the vicinity of the stone and close to the bed the extreme values of $|u'|$ can have the same order of magnitude as $|\overline{u}|$ so the fluctuating parts of drag and lift forces are of important for the entrainment of stones.

From Equation 2.1 and Equation 2.2 it can be inferred that:

$$F_D' \propto 2\overline{u}u' + u'^2 - \overline{u'^2} \tag{2.3}$$

$$F_L' \propto 2\overline{u}u' + u'^2 - \overline{u'^2} \tag{2.4}$$

For the fluctuating part of the lift force another relation was also proposed (Hofland, 2002; after Radecke & Schulz-DuBois, 1988):

$$F_L' \propto a\overline{u}u' + b\overline{u}v' \tag{2.5}$$

in which a and b are coefficients. The second term in the right hand side accounts for the vertical force component which is caused by the vertical velocity.

In the threshold condition, the fluctuating part of the drag and lift forces are expected to play an important role in dislodging stones on the bed.

Xingkui and Fontijn (1993), in their backward-facing step (BFS) experiments, found an increase of C_D for growing distances from the step. The drag coefficient in their experiments was determined by using the mean of the measured horizontal velocities. In BFS flow conditions, the fluctuating parts of horizontal velocities are high and can attribute largely to the instantaneous drag force and hence the mean drag force. Therefore, using mean velocities is not a proper choice. Let's find the drag coefficient for the experiment if instantaneous velocities are used:

$$\overline{F_D} = \frac{1}{2} C_D A_D \rho_w \overline{u^2} \tag{2.6}$$

$$\overline{F_D} = \frac{1}{2} C_D A_D \rho_w \left(\overline{u}^2 + \sigma_u^2\right) \tag{2.7}$$

The drag coefficient determined by Xingkui & Fontijn (C_{dxf}) is expressed as follows:

$$\overline{F_D} = \frac{1}{2} C_{dxf} A_D \rho_w \overline{u}^2 \tag{2.8}$$

From Equation 2.7 and Equation 2.8 we have:

$$C_{dxf} = C_D \left(1 + r^2\right) \tag{2.9}$$

As mentioned above, C_D can be considered a constant and does not depend on the flow conditions. Hence, the observed increase of drag coefficient C_{dfx} with the distance from the step is not in line with the decrease of the relative turbulence intensity r in the streamwise direction downstream of the reattachment point. Perhaps that was caused by the fact that not all horizontal forces that were measured by their dynamometer are covered by Equation 2.1. Some horizontal forces may have been caused by turbulence wall pressure (TWP) originating from turbulent structures that did not affect the velocities in the vicinity of the dynamometer.

2.2 Turbulence wall pressures (TWPs)

Quasi-steady forces can be considered the main causes of entrainment of stones. However, in turbulent flow, turbulence wall pressures can be a possible cause of entrainment. TWPs are pressures on a wall caused by the turbulence in a flow. TWPs at a certain location in an incompressible fluid are the sum of all velocity fluctuation gradients in the fluid domain. The intensity of TWPs induced by a single source of turbulence does decrease with the distance from the wall (Hofland, 2002).

The horizontal and vertical pressure gradient can be expressed in the following expressions for the fluctuating drag and lift force induced by TWPs (Hofland, 2002):

$$\Delta p'_D \propto F_x = -V\frac{\partial p}{\partial x} \propto v'\frac{\partial U}{\partial y} + \frac{Du'}{Dx} \tag{2.10}$$

$$\Delta p'_l \propto \rho\frac{Dv'}{Dt} \tag{2.11}$$

The second term on the right hand side of Equation 2.10 and the right hand side of Equation 2.11 cannot be evaluated from the present measurement.

Small-scale vortices can be important sources of turbulence wall pressure fluctuations. This TWP decreases rapidly at a certain distance from the vortex, so only vortices close to the stone can be expected (Hofland, 2002). It is believed that only vortices with the size of the order of the stone diameter will give significant forces on a stones and that a vortex at $0.5 - 2d$ above the stone will induce a large (lift) force. When a vortex passes the stone, the total vortex-induced force vector rotates clockwise from the lift direction to the drag direction. This lift-drag combination could be efficient in starting the movement (Hofland & Booij, 2004).

2.3 Force-generating mechanisms

Hofland & Booij, 2004 distinguish two force-generating mechanisms that may be responsible for the entrainment of stones: quasi-steady force fluctuations (QSF), caused by large-scale motion ($u' > 0$, and usually $v' < 0$); and small-scale turbulence wall pressure fluctuations (TWP), caused by small-scale wall-normal fluctuations (v') and vortices. In these two mechanisms, the latter was newly proposed by Hofland.

To quantify the influence of this force generating mechanism Hofland (2004) averaged the instantaneous horizontal velocity in the PIV recordings over a relatively large area A above the target stone, yielding $< u >_A$, and regard the values of $F_A \propto |< u >_A| < u >_A$ and its fluctuations. To identify the presence of this force-generating mechanism, Hofland (2004) regard the instantaneous standard deviation of v in area B near the target stone, $\sigma(v)_B$. This value becomes large when a vortex is present, and is not sensitive to the exact position of the vortex. To find the position of the vortex, swirling strength (λ) should be used (Adrian, Christensen, & Liu, 2000; Hofland & Booij, 2004). In short, if the respective quasi-steady forces or TWP are important, the indicators F'_A and/or $\sigma(v)_B$ will have high values. The combination of these indicators for all flow field was plotted to exam this judgement.

It is believed that not only must the magnitude of the forces be high but also the duration of time these forces acting on stones should be long enough to make stones move. With a relatively high value of force but lasts in a short time is not sufficient to dislodge stones on bed. To take the duration of time the forces acting on the stone into account, time-averaged values should be used.

In this report, time- and spatial-averaged velocity is used to investigate the influence of these force generating mechanisms. However, the problem is that how long the duration should be taken into account, 0.1, 0.2 or 1 second? We do not know exactly how long the extreme forces act to move the stone. A good way to determine this is that several values for the durations of time were tried, and the one that caused the most pronounced distinction of extreme values of F'_A and $\sigma(v)_B$ was chosen. In the same way, the averaging areas A and B were chosen.

Chapter 3

Experimental set-up

3.1 Introduction

The backward-facing step experiments were conducted in an open-channel flume which has a length of approximately 24 meters, a width of 0,495 meters. These were especially designed for PIV-experiments.

In the experiments, several areas downstream of the BFS where fluid velocities were obtained by means of the PIV technique were chosen. These measuring areas cover about 15 cm x 15 cm directly above the target stone in the center line of the flume, denoted by B001-B010 in the same order as they were conducted.

The first 5 tests (B001-B005) were conducted in which the discharge was increased in order to get the flow condition caused the target stone to move. During B006 (at the same position with B005), the movement of the target stone occurred. After B006, several locations were searched at which movements of the target stone occurred under the same flow conditions. From the experiments, the location of B009 was the place satisfied this and the locations of B007 & B008 were still too close to the BFS for movement of the target stone in the positive x-direction to take place.

In short, of the ten measurements only B006 and B009 were the ones with identical flow conditions in which the target stone was entrained. B003-B005 tests were conducted at the same location as B006 but with different flow conditions. In B005, a different target stone was used as well. B001 and B002 were conducted at

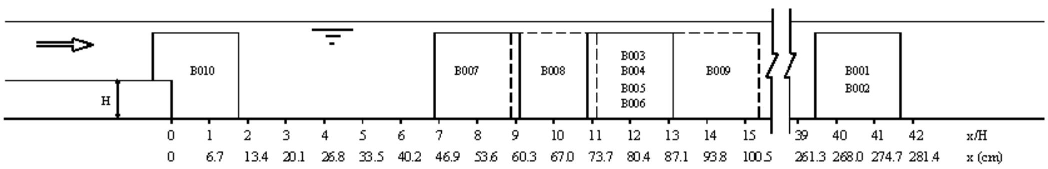

Figure 3.1: Overview of locations of measuring areas

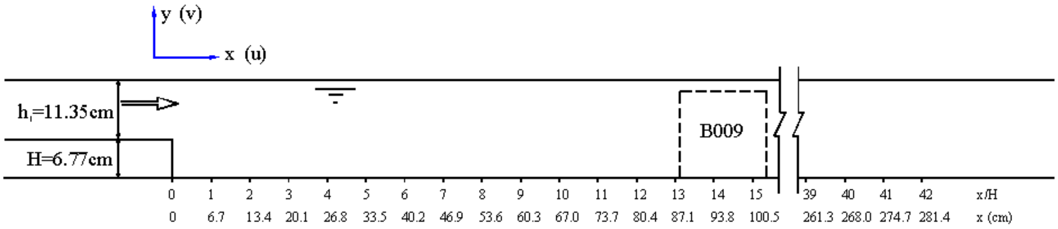

Figure 3.2: Side view of the BFS

the same location relatively far downstream of the BFS. In these cases, there were no movements of the target stone. The B009 experiment is described as follow.

3.2 The target stone

As the movement of stone in the bed is arbitrary due to the irregularities of natural stones, it is difficult to investigate the flow structure responsible for entrainment of stones. To solve this problem, the experiment only focussed on the movement of a single stone, the target stone. This makes it possible to capture the flow field above the stone at the moment of entrainment.

The actual stones with a nominal diameter, d_{n50}, of 17.8 mm were used to construct the bed material. However, the flow conditions produced in the experiments are not enough to move the stones. That's why the target stone made of epoxy resin having a density,ρ_S, of 1300 kg/m^3 was used. It had a d_n = 18.6 mm and curry shape factor of 0.62. As the main mode of movement of stones is pivoting (Hofland, 2003; after Carling *et al*, 1992), the target stone was placed on a hinge so that the motion is the same as in the prototype situation.

3.3 Flow parameters

The flow in the experiment had a discharge of $33.2 l/s$ and a water depth at $50 cm$ upstream of BFS (h_1) of $0.1135m$. The mean bulk velocity at upstream of BFS (U_1) can be determined as:

$$U_1 = \frac{Q}{Bh} = \frac{33.2 \times 10^{-3}}{0.495 \times 0.1135} = 0.590(m/s) \tag{3.1}$$

And the Reynolds number:

$$R_e = \frac{Uh}{v} = \frac{Q}{Bv} = \frac{33.2 \times 10^{-3}}{0.495 \times 1.01 \times 10^{-6}} = 66400 \tag{3.2}$$

From Equation 3.2 it can be seen that the Reynolds number is constant along the flume. The Froude number can be obtained as follow:

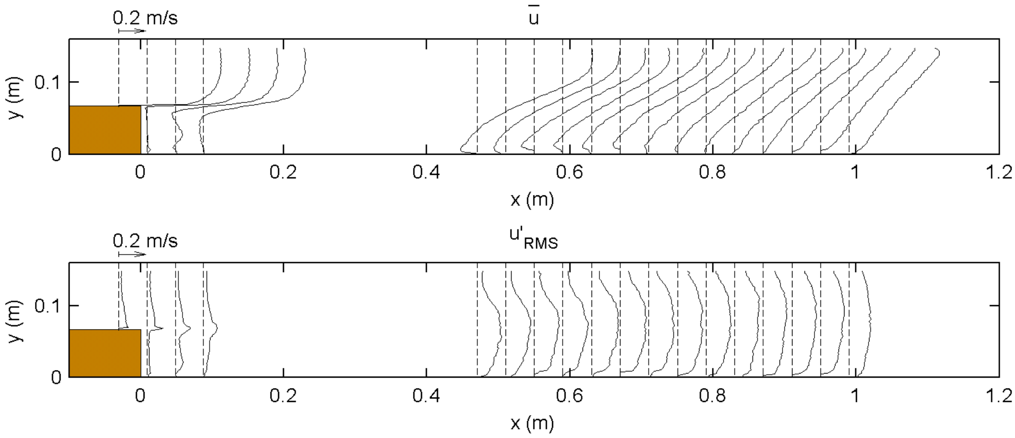

Figure 3.3: Upper plot: profiles of mean longitudinal velocity. Bottom plot: root mean square value of longitudinal velocity fluctuations. The distance between two consecutive cross-sections for which profiles are plotted is fixed (De Ruijter, 2004).

$$F_r = \frac{U}{\sqrt{gL}} = \frac{0.59}{\sqrt{9.81 \times 0.1135}} = 0.56 \tag{3.3}$$

At 500 cm downstream of BFS, the water depth is 17.82 cm. We have:

$$U_2 = \frac{Q}{Bh} = \frac{33.2 \times 10^{-3}}{0.495 \times 0.1782} = 0.376(m/s) \tag{3.4}$$

Despite of the fact that at the measurement area the flow condition is still far more from uniform and Shield factor cannot be applied to estimate the mobility parameter of the stone, we still use Shield factor for a rough estimation. The flow parameters at the position of 500 cm downstream of BFS can be used to determine the mobility parameter (at such distance, $x/H = 74$, the flow condition can be considered uniform). An overview of the mean flow conditions of the experiments with peer flow conditions can be seen in Figure 3.3.

From Figure 3.3 it can be seen that a zone with negative velocities is visible near the bottom, stretching from x = 0 m to about x = 0.80 m. The measuring area of the B009 experiment is just behind this zone.

At 500 cm downstream of BFS, the "smoothness" coefficient can be determined as:

$$C = 18 \log \frac{12R}{k_r} = 18 \log \frac{12 \times 0.1782}{0.0178} = 37.4(\frac{\sqrt{m}}{s}) \tag{3.5}$$

in which R is the hydraulic radius, $R \approx h = 0.1782m$; k_r is the equivalent roughness, $k_r \approx d_{n50} = 0.0186m$. The shear velocity ($u_*$) is expressed as follow:

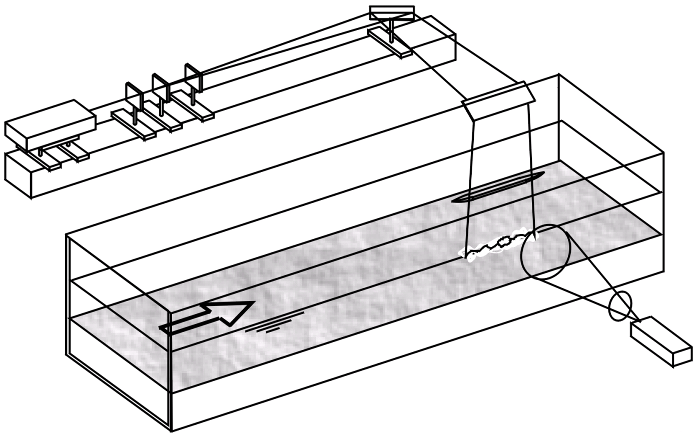

Figure 3.4: PIV set-up with laser (top left), sheet optics, mirrors, window on water surface and camera (bottom right) (Hofland & Booij, 2004).

$$u_* = \frac{U\sqrt{g}}{C} = \frac{0.376\sqrt{9.81}}{37.4} = 0.032(m/s) \tag{3.6}$$

The particle Reynolds-number, Re_*:

$$R_{e*} = \frac{u_* d_{n50}}{v} = \frac{0.032 \times 0.0186}{1.01 \times 10^{-6}} = 589 \tag{3.7}$$

And the mobility parameter, Ψ:

$$\Psi = \frac{u_*^2}{\Delta g d_{n50}} = \frac{0.032^2}{0.3 \times 9.81 \times 0.0186} = 0.019 \tag{3.8}$$

With $Re_* = 589$, from the Shield curve it can be inferred that the critical dimensionless shear stress,Ψ_c, equals 0.055. The mobility parameter (Shield factor) of the target stone in the experiment (see Equation 3.8) is far less than the critical value.

In this report x and y are the streamwise and upward coordinates respectively as depicted in Figure 3.2. The horizontal and vertical velocities are denoted as u and v. The time-averaged value of u is denoted as $\bar{u}$, the fluctuating part of u $(u - \bar{u})$ is denoted as u' and the spatial averaged u-velocity over area A is denoted as $< u >_A$.

3.4 Equipment

A La Vision PIV system (hardware and software) was used to measure streamwise vertical 2-D velocity fields in the center of the flume above the target stone(Figure 3.4). More details can be found in (Hofland & Booij, 2004; De Ruijter, 2004).

Chapter 4

Data processing

4.1 Introduction

The data obtained from the experiment include pressure measurement and series of images. In this report, only image data are chosen to deal with.

In the experiment, three kinds of PIV recordings were made to capture the flow field around the target stone. The first recordings consisted of series of images containing the flow field around the stone before and after the stone movement. The maximum possible sample rate, 15 Hz, was chosen to make these recordings. So every 0.067 (1/15) second a flow field was stored. Generally, in each event (the target stone moved) 55 images were capture. This means that the total time of recording each event is 3.6s (the number of intervals (54) multiplied by the interval time (1/15s)). These image recordings are used to inspect the flow field around the target stone by making the conditionally averaged velocity fields and instantaneous velocity fields.

The second recordings were also made to capture the flow field around the target stone and were used to calculate average values of the velocities. This time, the stone was stuck to the bed so that it could not move. The recordings were made with a sample rate of 0.5 Hz for 10 minutes (300 images). The stone did not move so the flow field was not disturbed as it was in the case the stone moved. Also the time of measurement was long enough (with respect to the characteristic time scale of the turbulent motion) to be used to calculate the average values of the velocity components.

The third and last recordings were also made with the sample rate of 15 Hz as the first ones but this time the target stone was glued to the bed as the second. The maximum 300 images were captured with the total time of 20 seconds. These recordings, among other things, are supposed to be used to investigate if quasi-periodic mechanisms were present. In this report, these data are not used. The main procedures of data processing are shown in Figure 4.1.

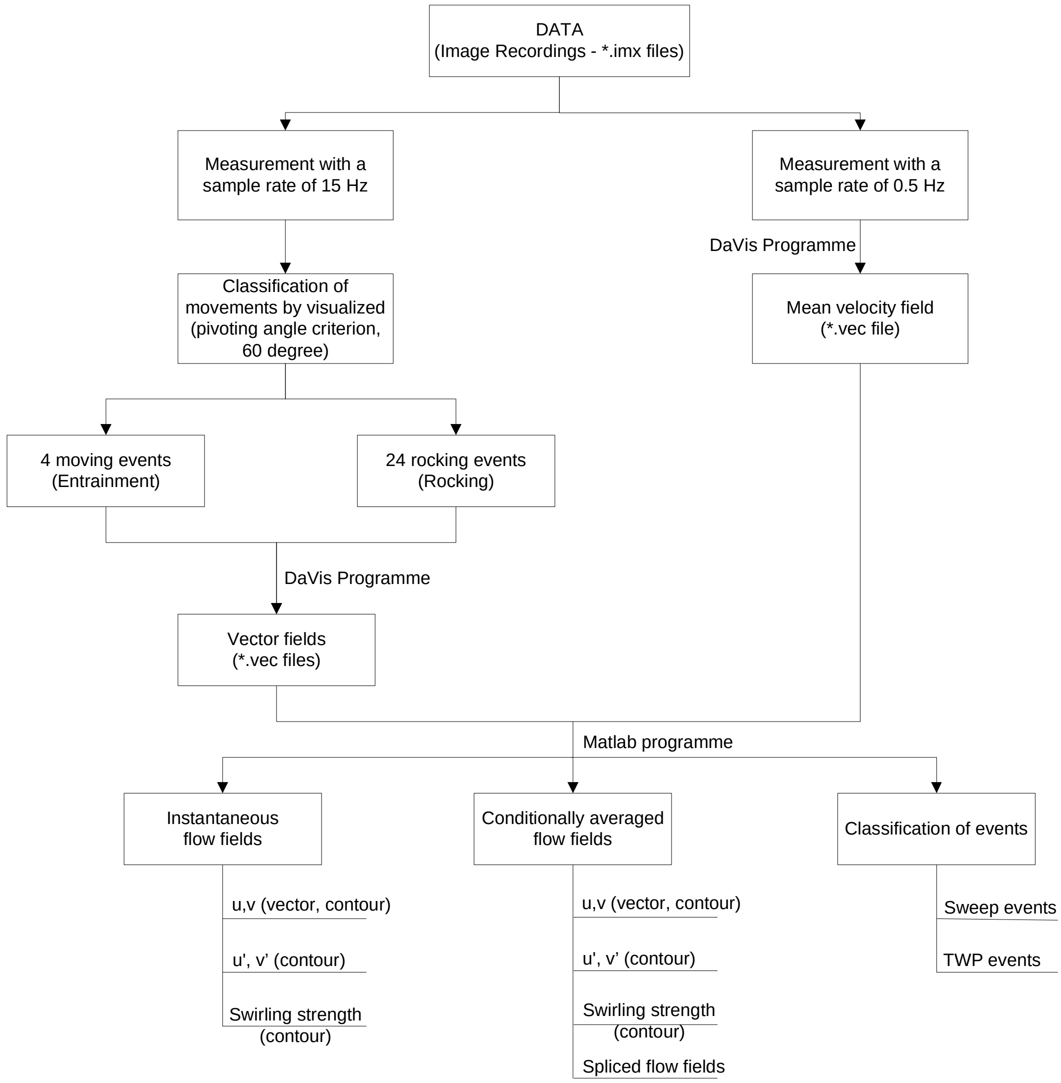

Figure 4.1: Procedures of data processing.

4.2 Visualized classification of events

The Davis programme is used to inspect all 1485 images of the first type recordings to determine the events in which the target stone moved. We discern two modes of motion of the target stone, rocking and entraining. The stone was assumed to be entrained (i.e removed from its pocket) if it pivoted around the pivoting point at an angle larger than 60^0. Otherwise the mode of movement was regarded as rocking.

Four entrainment and 24 rocking events were found in the B009 data. For each event, 25 frames before and 25 frames after the movement were collected. With 4 entrainments we had 100 image-files, numbered from 1 to 100. In this way, files 25, 75, 125, 175 were the images of the flow fields just before the movement of the four entrainment events respectively. From now on, we call these four entrainments event #25, 75, 125 and 175.

4.3 Inspection of vector plots

It can be difficult to distinguish the flow structures in an instantaneous flow which has large gradients. Therefore decomposition methods have been used to interpret velocity field. Adrian et al. (2000) give an overview of methods of analyzing and interpreting velocity field data. Each method has its own strength and weakness and is suited for a particular investigation. For example, Reynolds decomposition is a good way for analyzing statistics but is not always the best way for visualizing the turbulent mechanics of a flow. In this report, two decomposition methods have been used: the Reynolds decomposition and the Galilean decomposition.

The vortex, one of the most important flow structures that is expected to represent in the flow field in our experiment, can be defined as: "A vortex exists when instantaneous streamlines mapped onto a plane normal to the core exhibit a roughly circular or spiral pattern, when viewed in a reference frame moving with the center of the vortex core". From this definition it can be inferred that to recognize vortices embedded in large-scale motion one must subtract a constant convection velocity from the whole velocity field. This decomposition of the velocity field is known as Galilean decomposition.

It can be seen that if the convection velocity to be subtracted equals the velocity of the core of a vortex, the vortex can be the most recognizable. However, to detect a vortex and pinpoint its location it is not necessarily to subtract the exact convection velocity. In these cases, the velocity vector pattern is not completely circular (Adrian et al., 2000). To identify the majority of the turbulence eddies, one should consider a range of convection velocity (U_c). In general, the convection velocity can be chosen as a fraction of the bulk velocity (U_{bulk}) (De Ruijter, 2004). In this report, the convection velocity $U_c = 0.8 \times U_{bulk}$ is found to unveil the most turbulence eddies.

Although the Galilean decomposition is a good method to identify vortices, this method still depends more or less on the frame reference (convection velocity). Another method of vortex identification which does not depend on the frame reference is the swirling strength. The swirling strength is a measure of the intensity of the local rotation in a flow field. It is capable of pinpointing separate vortices accurately (Adrian et al., 2000; Hofland & Booij, 2004). In this report, the swirling strength is plotted in the same figure with velocity vector pattern. In conditionally averaged flow fields, it can be seen that the vortex is not much circular and the high swirling strength does not locate exactly at the center of the vortex. However, when the vortex reaches closely to the stone, the swirling strength becomes more intense and concentrated at the center of the vortex.

In the Reynolds decomposition, the time-averaged velocity of each location is subtracted from the corresponding instantaneous velocity. This is the traditional method of decomposing a turbulent velocity field. This method tends to unveil more vortices than any single Galilean decomposition because the vortices frequently move at velocities close to the local mean velocity. A drawback of Reynolds decomposition is that it removes large-scale features that are associated with the mean flow such as large regions of relatively uniform momentum.

4.4 Splicing

Because the measuring area was too small ($15 \times 15cm$) to inspect the large-scale structure directly, a hybrid technique was used to merge a sequential series of PIV recordings.

This technique will be called splicing here. This technique is described in (Hofland & Booij, 2004) as: "To this end first the correlation of the upstream part of the outer u' field of the first image and an equally sized downstream part of the outer u' field of the second image was determined as a function of the overlap length. The overlap at which this function was maximal was taken as the (instantaneous) value of the convection velocity of the total flow structure. Subsequently a new flow field is created by averaging the velocities of the overlapping part of the two images, and adding the remaining parts on both sides. This total image is now used as the first image and the third image from the series as the second. This process is repeated for all recordings during the measurement of a single event. The resulting image can be seen both as a spatial image and as a temporal image with a direction opposite to the spatial image."

Chapter 5

Experiment Results

5.1 Classification

As aforementioned, at the time the stone starts to move the two force-generating indicators are expected to have high values. We plotted the combination of the values of the two indicators just before the time the movement of the stone for all flow fields. Several size of A and B were tried to find the most pronounced distinction of extreme values of the indicators. The final sizes of A and B are depicted in Figure 5.1.

It can be seen that the area B is larger than the area A. The width of the area B is the same size of the vortex and this area covers the whole vortex just before the movement. As can be seen later on this section, the area A is the same size with and covers the fluid package with relatively high u-velocity fluctuation (u').

The combination of the force-generating indicators at the time just before the movement (instantaneous values) and at the measurement with a fixed stone is depicted in Figure 5.2. It is clear that the values of force-indicators at the time of entrainment are high. In some events, both F'_A and $\sigma(v)_B$ are high while in others, if one indicator is high, the other is low. We will call values of large F'_A sweep events, and with large $\sigma(v)_B$ TWP events (after Hofland & Booij, 2004). Events with both F'_A and $\sigma(v)_B$ are high or low are named transition. For most events, F'_A is positive. It means that to make the stone move, the longitudinal velocity must be increased.

As mentioned above, we expect the duration of time the forces acting on the stone will play a role in the entrainment so we regard here the time-averaged values of the force-generating indicators. It is hoped that by averaging the values of the indicators over the time we can get more pronounced distinction of the extreme values, especially the values in the moving events and the values in slow measurement. Unfortunately, the sample rates of these two measurements are different. The interval between two sequential frames in slow measurement is 2 seconds while this interval in 15 Hz measurement is 0.067 seconds. For this reason, we cannot compare the averaged force-indicator values of both measurements with different durations

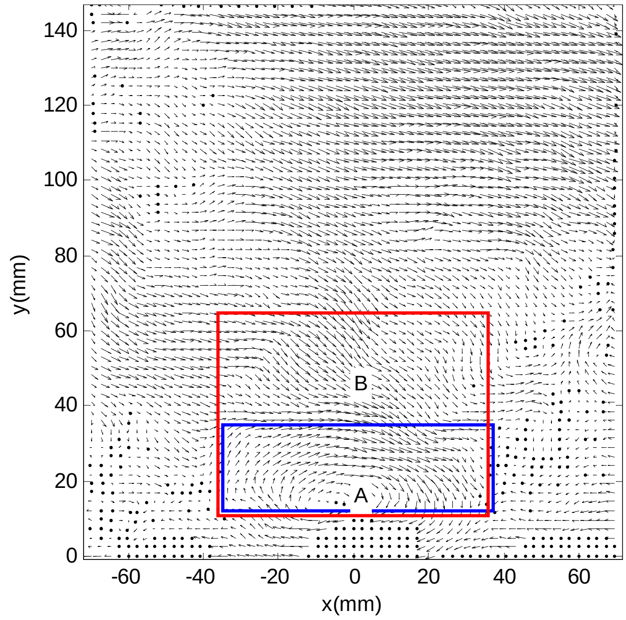

Figure 5.1: Areas used for averaging. The target stone is located at (x,y)=(0,0).

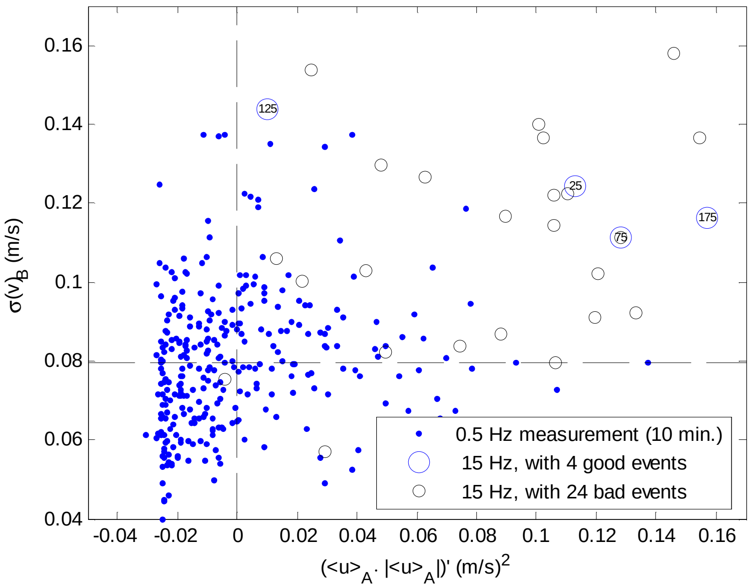

Figure 5.2: Classification of events. F'_A ($| < u >_A | < u >_A$) and $\sigma(v)_B$ indicate quasi-steady and TWP forces respectively. Dots are the values of a 10 min. / 0.5 Hz measurement with a fixed stone. The circles are the values just before stone movement.

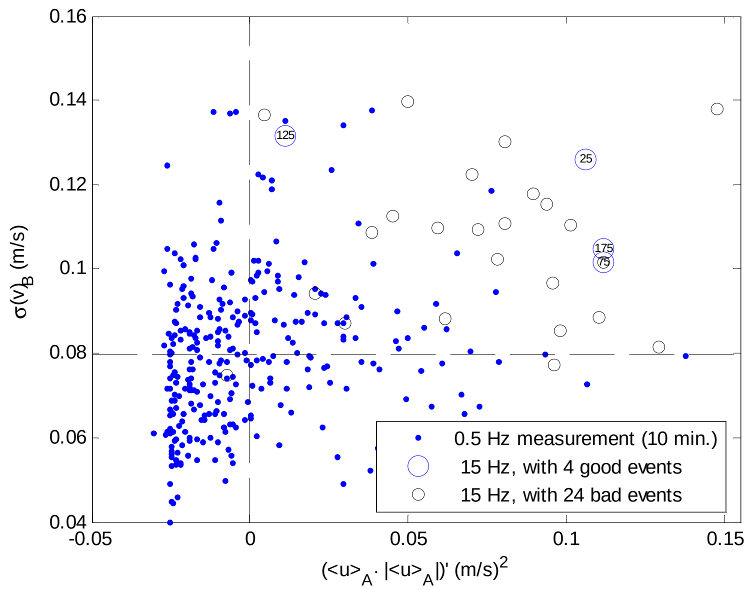

Figure 5.3: Classification of events. F'_A ($| < u >_A | < u >_A$) and $\sigma(v)_B$ indicate quasi-steady and TWP forces respectively. Dots are the values of a 10 min. / 0.5 Hz measurement with a fixed stone. The circles are the averaged values over 3 frames before and 1 frame after movement.

of time.

In the next step, we will plot the combination of the indicators for both the slow measurement and the flow field around the movement. This time, the values for slow measurement are the instantaneous spatial values while the values for flow field in the movement measurement are the spatial- and time-averaged values.

The averaged values of the force-indicators can be obtained by averaging the instantaneous values of the indicators at some frames around the time of the movement of the stone. It is obvious that the forces acting on stones before the movement are very important in dislodging the stones. However, the forces acting on the stones during the entrainment are also expected to play a role. In general, several numbers of frames before (N_{fb}) and after (N_{fa}) the movement are chosen to average. Give N_{fb} the values from 1 to 4 and N_{fa} the values from 0 to 3 we have 16 combinations of the averaged values. The combination that gives the most pronounced distinction of the extreme values is depicted in Figure 5.3 ($N_{fb} = 3$ and $N_{fa} = 1$).

The force-indicators at different time around the entrainment of an arbitrary sweep event and an arbitrary TWP event are depicted in Figure 5.4 and Figure 5.5.

It can be seen from Figure 5.4 that for a sweep event, the values of $\sigma(v)_B$ do not change much but the values of F'_A vary highly in time. At 5^{th} frame before the entrainment (0.3s), $F'_A \approx 0$. The values of F'_A increase rapidly and reach the highest values at the time just before the entrainment. After the stone started to move,

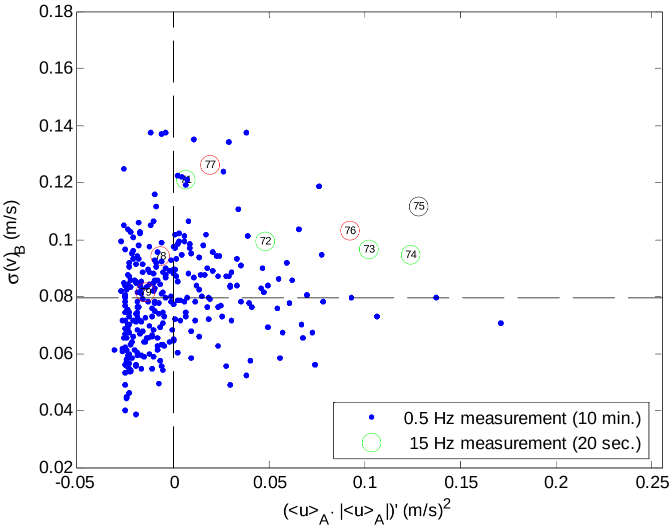

Figure 5.4: Force-indicators at different time around the entrainment of sweep event #75.F'_A ($| < u >_A | < u >_A$) and $\sigma(v)_B$ indicate quasi-steady and TWP forces respectively. Dots are the values of a 10 min. / 0.5 Hz measurement with a fixed stone. The circles are the instantaneous values at frames around the entrainment (5 frames before and 4 frame after movement).

these values decrease more rapidly and nearly reach to zero after 2 frames.

In the TWP event as shown in Figure 5.5, an inverse situation can be found. The values of F'_A do not change very much and nearly reach to zero. The value of $\sigma(v)_B$ at the 5^{th} frame before the entrainment is also quite low. But in time, these values become larger and reach to a relatively high value at the time just before the entrainment of the stone. After the time the stone started to move, this value keeps high for a while and then decreases rapidly.

It can be concluded that in sweep events, the increase of F'_A is correlated with the entrainment of the stone while in TWP events, $\sigma(v)_B$ plays a role.

5.2 Conditional averages

We first regard the conditionally averaged flow field then if a certain flow structures are present, we can check afterwards whether these structures can be recognized in the instantaneous fields as well.

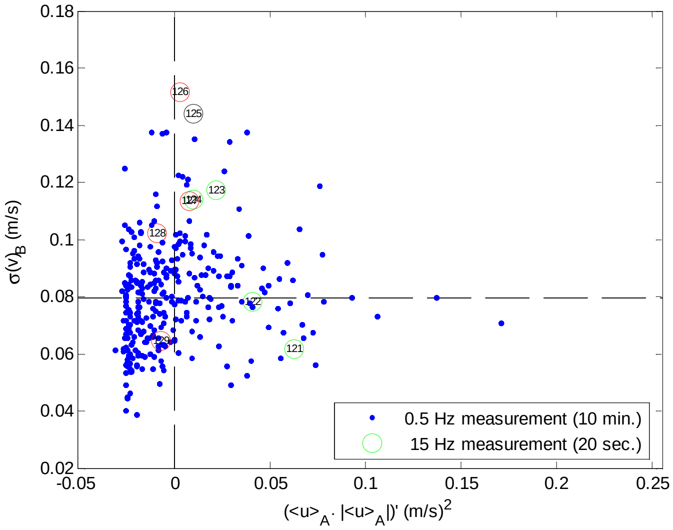

Figure 5.5: Force-indicators at different time around the entrainment of sweep event #125.F'_A ($| < u >_A | < u >_A$) and $\sigma(v)_B$ indicate quasi-steady and TWP forces respectively. Dots are the values of a 10 min. / 0.5 Hz measurement with a fixed stone. The circles are the instantaneous values at frames around the entrainment (5 frames before and 4 frame after movement).

5.2.1 Small-scale conditionally averaged flow structures

Decomposed flow fields

The conditionally averaged sequences of all events (moving and rocking events) are used to investigate the flow structures around the time the movement of the stone (4 frames before and 1 frame after the stone really up). The contour plots of conditionally averaged u' and v' (Reynolds decomposition) are depicted in Figure 5.6. Figure (5.7 shows the vector plots of the conditionally averaged flow fields (Galilean decomposition). In the Galilean decomposition, the convection u-velocity of $0.8 \times U_{bulk}$ is found to give the most pronounced distinction of the vortex.

For the entrainment events in Figure 5.6 we can see that a fluid package with the increased u-velocity moves both from the left to the right and from the top to the bottom. This fluid package moves toward the stone with a horizontal velocity of approximately $0.34 m/s$. At the time just before the movement, it nearly hits the stone. In the v'-plots a smaller fluid package with high v-velocity near the bed moving from the left to the right can be seen. This package is embedded in a large area with negative fluctuating part of vertical velocity.

Accompanied by the increased u-velocity fluid package is a clockwise vortex which can be seen in Figure 5.7. This vortex also moves from the left to the right and from the top to the bottom. It nearly hits the target stone at the time the

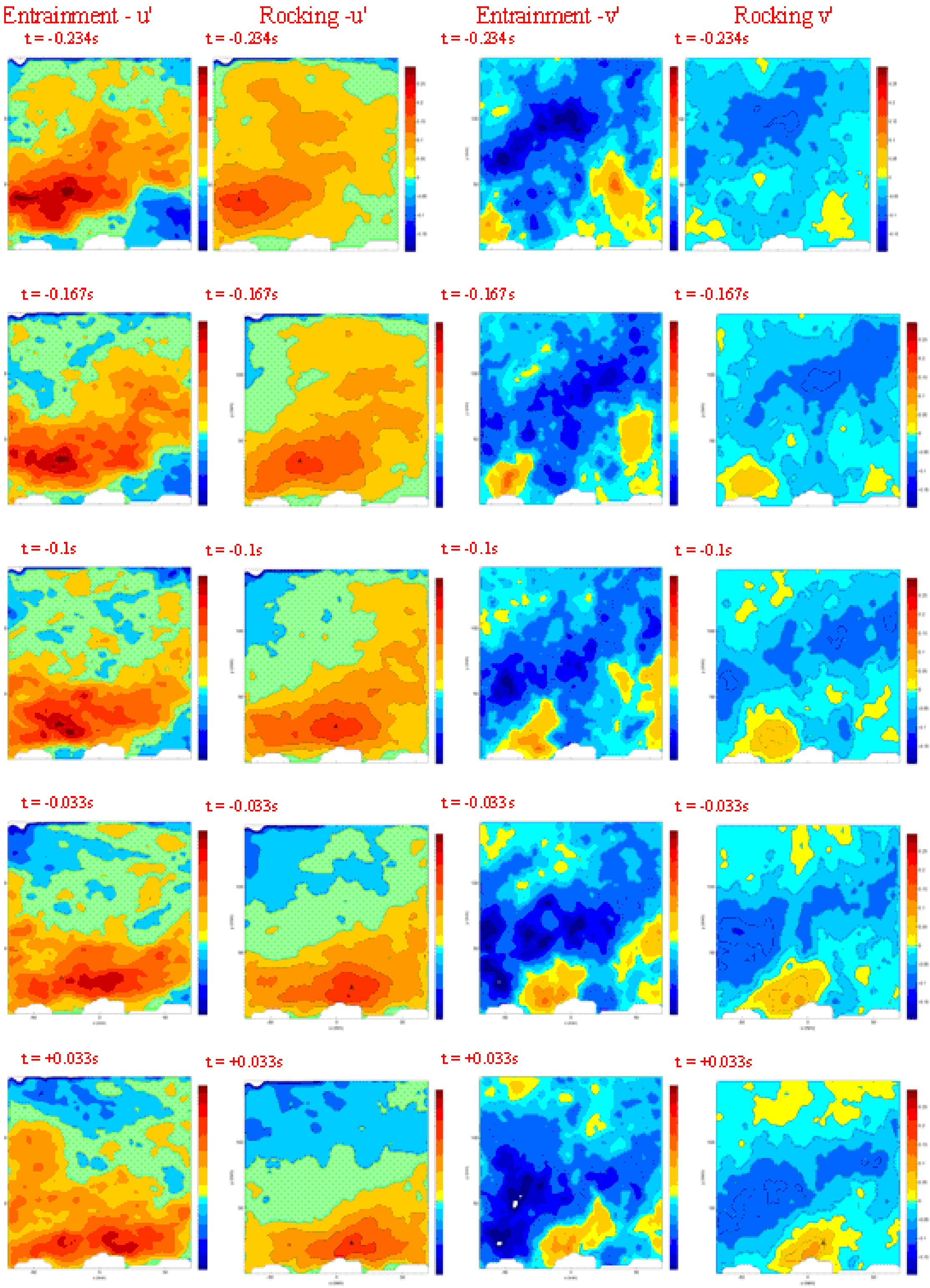

Figure 5.6: Sequence of conditionally averaged flow fields of the entrainment and rocking events. The first two columns are u'-plots of entrainment and rocking even respectively. The last two columns are u'-plots of entrainment and rocking even respectively. The target stone is located at x = 0 and starts to move at t = 0.0s.

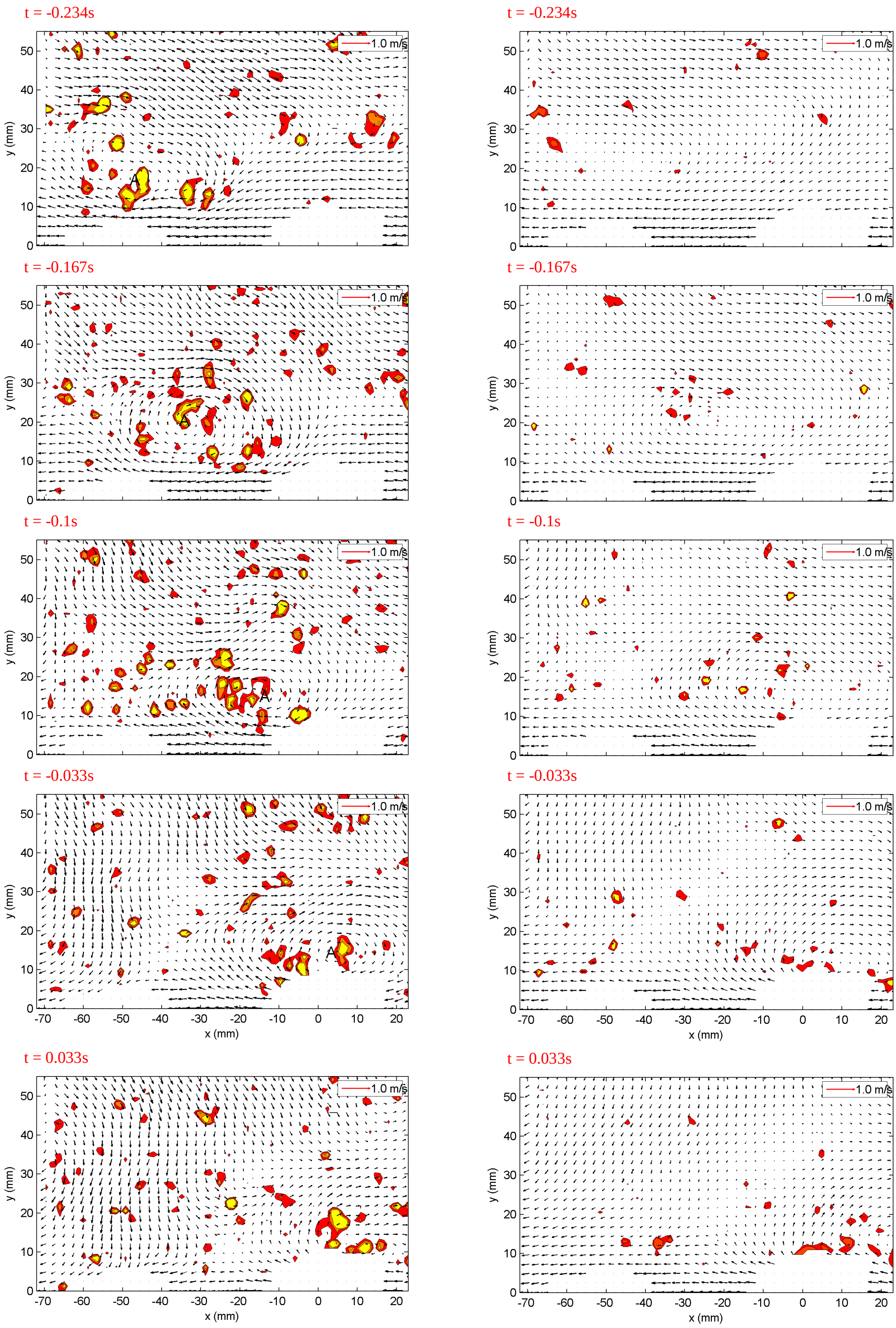

Figure 5.7: Sequence of conditionally averaged flow field of the entrainment and rocking events: vector plot of $u - 0.8U$, shading: $\lambda_{ci}^2 > 100, 175, 250s^{-2}$. Right: entrainment events and left: the rocking events. The stone is located at x = 0 and starts to move at t = 0.0s.

stone starts to move. It can be seen that the vortex seems to move with the same velocity as the fluid package and always leave the package behind. After the vortex reaches the stone, the fluid package with the increased u-velocity follows and hits the stone. When coming close to the stone, the vortex becomes more concentrated and intense. The size of the vortex has the same order with the size of the stone and is located at a distance of $0.5 - 2d$ from the stone.

In the rocking events in which the target stone did not really pivot but just rocked in its pocket, conditionally averaged flow field have also been made to be compared with the moving events. From Figure 5.6 and Figure 5.7 it can be clearly seen that the same situation can also be found in the rocking events. The difference is that in rocking events, the flow structure is less intense. In the rocking events, the vortex is not much clear and also less intense.

Non-decomposed velocity fields

The non-decomposed conditionally averaged velocity fields of both moving and rocking events are depicted in Figure 5.8. From the pictures that present u-velocity we can see an exchange of momentum in the flow field. The region with high u-velocity of the upper part of the flow spreads out toward the bottom. In the entrainment events, some fluid packages with high momentum separate from the upper part and move toward the bed. In the rocking events, the high momentum fluid areas are located at the higher parts compared to those in the entrainment events. Near the bottom, the horizontal velocities also increase but are less intense than those in the former. In both cases, when the u-velocity near the bed becomes large, the velocity near the surface becomes less.

In the most part of the inspected area, the vertical velocities are negative. Only a small fluid package with high positive vertical velocities is found close to the bed. This package also moves from the left to the right toward the stone.

5.2.2 Large-scale spliced conditionally flow structure

In the experiment, only four events are found. Of the four, only two events are considered sweep event (event #75 & #175); one event TWP event (event #125) and the last the transition (event #25) (see Figure 5.3). That's why only conditionally averaged recordings for sweep events are depicted here in Figure 5.9.

The conditionally averaged sequences of sweep events show a large-scale ($\approx 2h$ in streamwise direction) area of increased longitudinal velocity. The shape and size of the sweep are not much similar to those in uniform flows identifies by Hofland and Booij (2004) and by Buffin-Belanger et al (Hofland & Booij, 2004; after Buffin-Belanger *et al*, 2000).

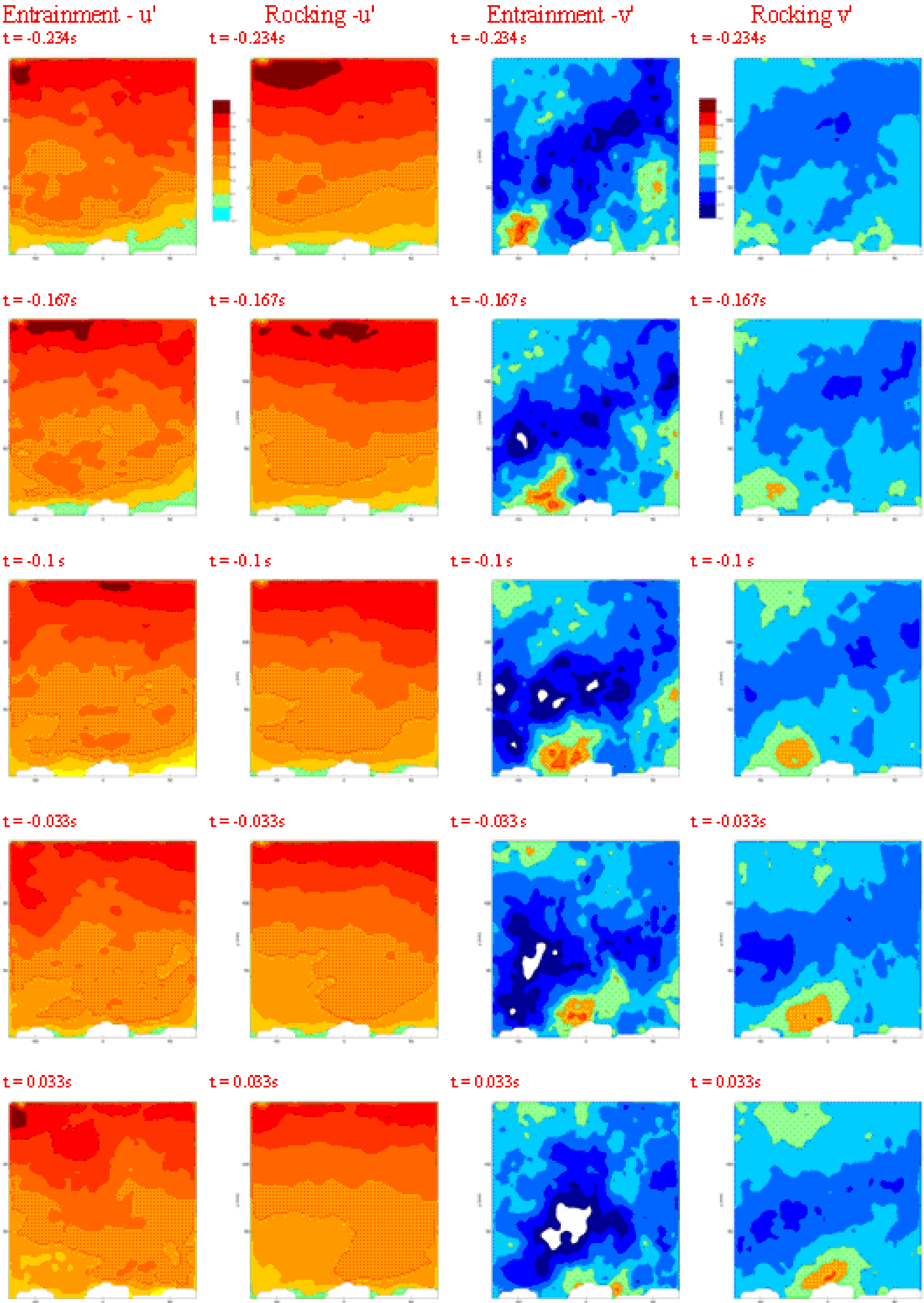

Figure 5.8: Sequence of conditionally averaged flow fields of both entrainment and rocking events at 4 frames before and 1 frame after the stone really up. The stone is located at x = 0 and starts to pivot at t = 0.0s.

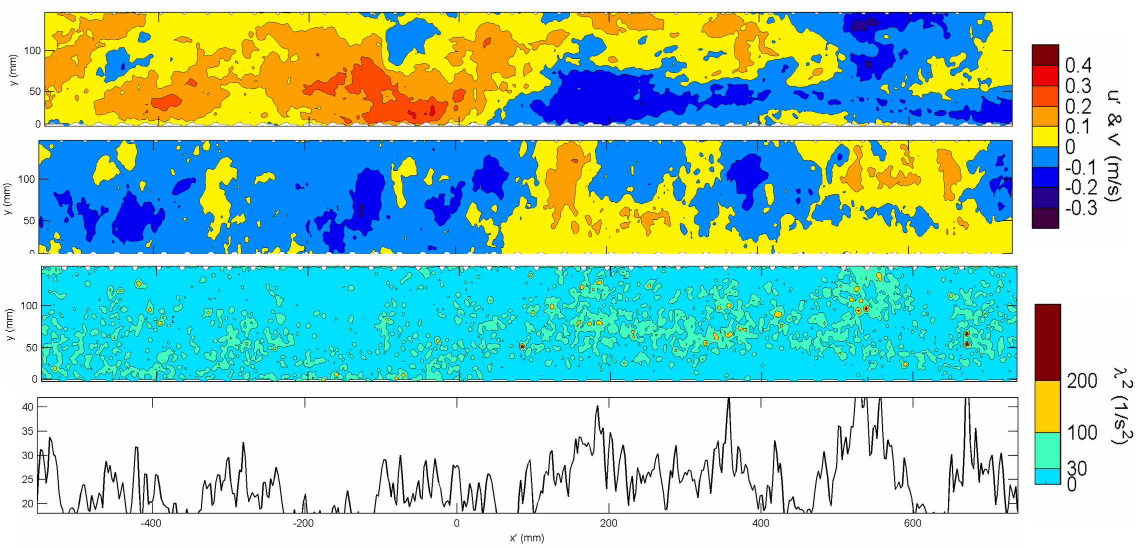

Figure 5.9: Large-scale spliced and conditionally averaged recording for sweep events. The stone moves at x=0. Top plot: u', second plot: v', third plot:λ_{ci}^2, bottom plot $< \lambda_{ci}^2 >_h$.

5.3 Instantaneous flow structure

5.3.1 Small-scale instantaneous flow structure

We will regard the small-scale flow structures with intense v fluctuations around the first movement of the target stone. Of the four entrainments, only in sweep events a single vortex rotating in the clockwise direction, moving toward the stone can be indeed visible. In these cases, the vortex is located right above the stone just before the entrainment (t = -0.033s). In the next frame (the frame just after the entrainment, t = +0.033s), this vortex moves little downstream and part of it seems to be "eaten" by the stone. This can be responsible for lifting the stone because it causes a low-pressure area under its core (Hofland & Booij, 2004).

In Figure 5.10 and Figure 5.11 several positions with high value of swirling strength can be seen. At these positions, a rotational flow field is indeed visible if the proper convection velocity is subtracted (Adrian et al., 2000; Hofland & Booij, 2004).

Another small-scale flow structure called a hairpin vortex packet can also be seen. Hairpin vortex packet (HVP) is a series of broad horseshoe/hairpin vortices, with the heads aligned at an angle with respect to the bed that cover an area of almost uniform low-momentum (Hofland & Booij, 2004 after Adrian et al., 2000). A clear HVP was visible in event #75 and # 125 (indicated by the dashed line in Figure 5.10 & Figure 5.11). In the HVP the velocity is slow down and directed upward.

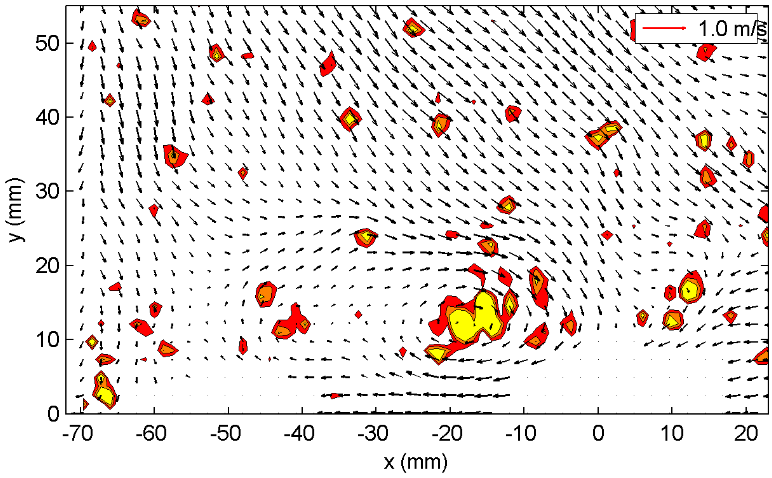

Figure 5.10: Detail of typical instantaneous flow field with single vortex before movement of the target stone. Vector plot of $u - 0.8U_{bulk}$ (event #75), shading: $\lambda_{ci}^2 > 100, 175, 250s^{-2}$.

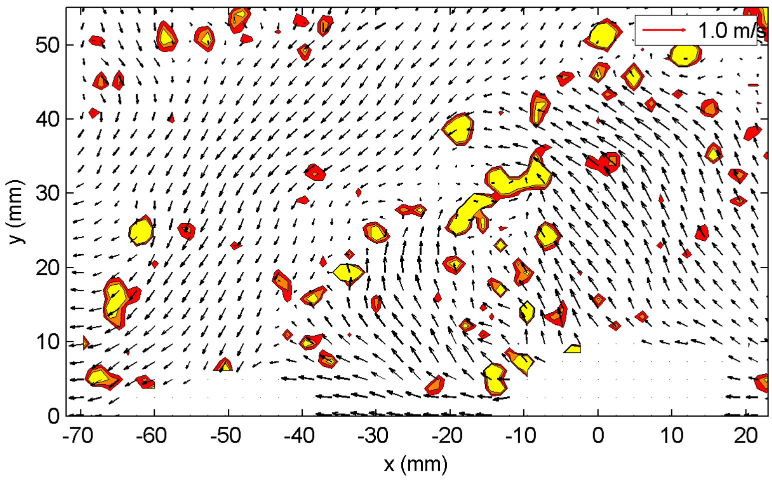

Figure 5.11: Detail of typical instantaneous flow field with small hairpin vortex packet before movement of the target stone. Vector plot of $u - 0.8U_{bulk}$ (event #125), shading: $\lambda_{ci}^2 > 100, 175, 250s^{-2}$.

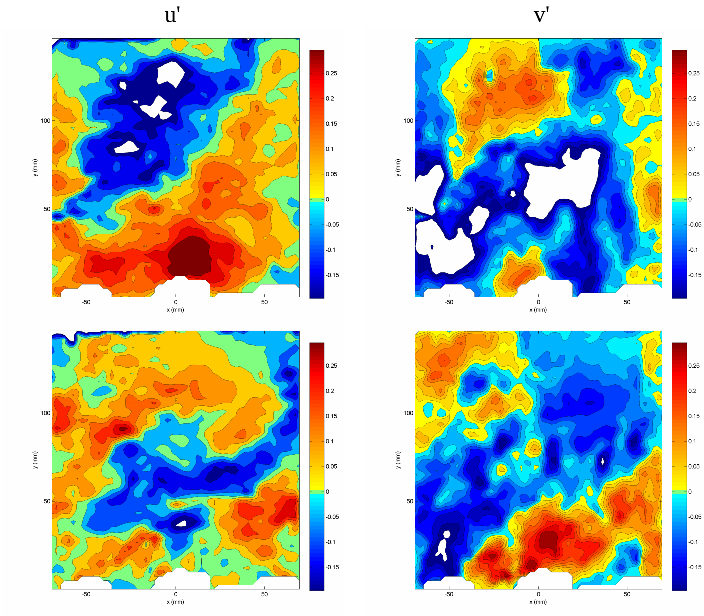

Figure 5.12: The instantaneous flow field just before the entrainment. Top row: event #75, bottom row: event #125.

The same situation found in conditionally averaged flow field can also be seen in the instantaneous flow field. At the time just before the entrainment, a fluid package with high velocities moves toward the stone. In sweep event, a highly increased u-velocity and slightly increased v-velocity can be seen. In the TWP event, v'-velocity is much intense while u-velocity is not very high (Figure 5.12). In all four events, a fluid package with increased v-velocity near the stone was found.

5.3.2 Large-scale spliced flow structure

The sweep event in Figure 5.13 (the same as in Figure 5.10) is similar to the conditional average of Figure 5.9. However, the length of the sweep is approximately $1.5h$, smaller than that in conditional average ($2h$). These sweeps do not have the wedged-shape and their length is half of that in the uniform flow as found in (Hofland & Booij, 2004). The length of the sweep in these data is similar to that of the B006 experiment (De Ruijter, 2004). Other differences between the conditional average and the instantaneous flows are that the values in the instantaneous flows are more intense and the gradient is also larger.

The TWP event in Figure 5.14 shows an increase of vertical velocity at the moment of entrainment. This is followed by a small sweep event. Over the length of the spliced plot there seem to be three HVPs, one of which includes the strong

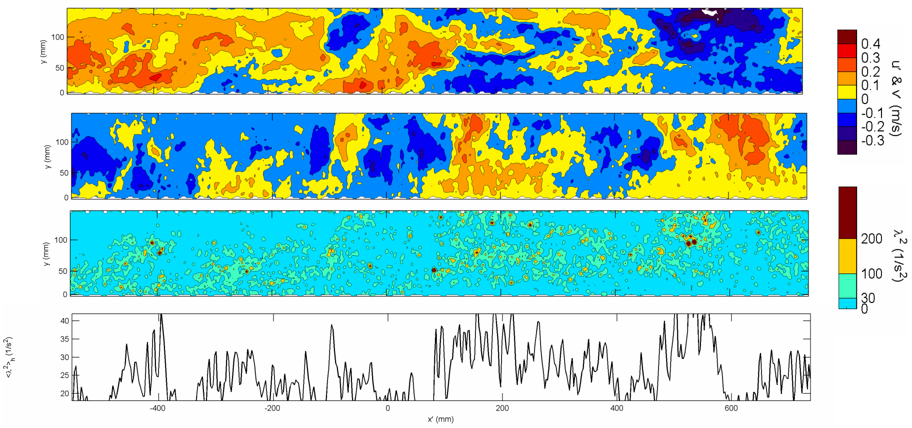

Figure 5.13: Large-scale spliced flow field of sweep event # 75, see also Figure 5.10. The stone moves at $x = 0$. Top plot: u', second plot: v', third plot: λ_{ci}^2, bottom plot $< \lambda_{ci}^2 >_h$.

vortex that moves the stone at $x = 0$ (Figure 5.11). These HVPs are indicated in Figure 5.14 by inclined dashed lines.

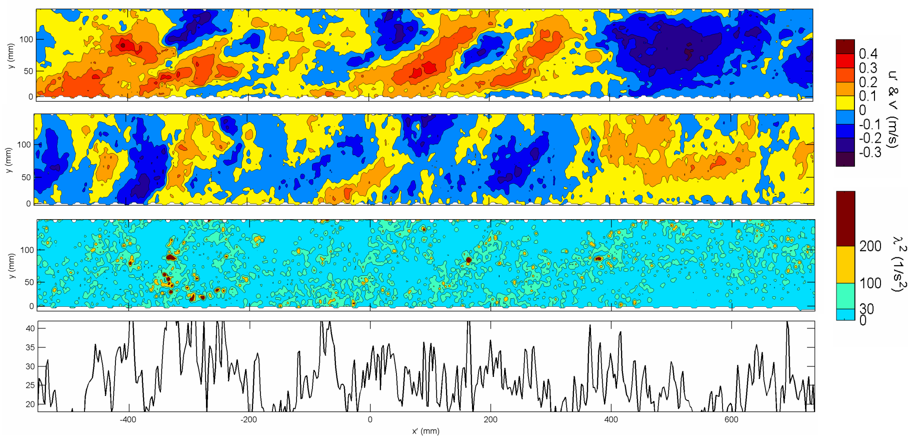

Figure 5.14: Large-scale spliced flow field of TWP event #125, see also Figure 5.11. The stone moves at $x = 0$. Top plot: u', second plot: v', third plot: λ_{ci}^2, bottom plot $< \lambda_{ci}^2 >_h$.

Chapter 6

Conclusions and recommendations

6.1 Discussion

Stones used for protection purposes often have sharp edges. Their smallest axis points upwards. This means that the exposed area for the lift force is usually larger than that of the drag force and the torque created by the drag force is not very large yet. To dislodge the stone, an increase of lift force is necessary. An increase of lift force will result in a high increase of the torque, making the stone pivot a little around the pivoting point and then the vertical exposed area of the stone becomes larger, making the torque caused by drag force increase rapidly. This combination of the increase lift then drag force is optimal for moving the stone from its pocket.

The combination of a large-scale sweep and an embedded small-scale ejection at the time of the entrainment which is found in previous experiments (Hofland & Booij, 2004; De Ruijter, 2004) is not clearly seen in these data. In the sweep events (Figure 5.9 & Figure 5.13), only a large-scale sweep is present at the time the stone started to pivot. Not a single small-scale ejection was found. However, in Reynolds decomposed flow field as showed in Figure 5.6 and Figure 5.12 we do see an area near the stone with high positive u' and v' (outward interaction). This small-scale structure disappears in large-scale spliced flow field (Figure 5.9 and Figure 5.13). This may be due to the fact that in the splicing, we only do the correlation of u' then the averaged values of v' become negative.

In the TWP event (Figure 5.14) both *outward interaction* ($u' > 0$ & $v' > 0$) and *sweep* ($u' > 0$ & $v' < 0$) were present, first came the *outward interaction* then came the *sweep*. The sweep in TWP event was not close to the bed and also less intense than in the sweep event. In this case, the vertical fluctuations initiate the motion of the stone and the sweep moves the stone further over its pivot point. The sweep does not to have to be very high to move the stone because the vertical exposed area increases after the first lift, making the torque caused by drag force increases rapidly. This combination of *outward interaction* and *sweep* can result in an *outward interaction* as depicted in Figure 6.1.

In the two sweep events, the large sweep causes a significant increase of quasi-

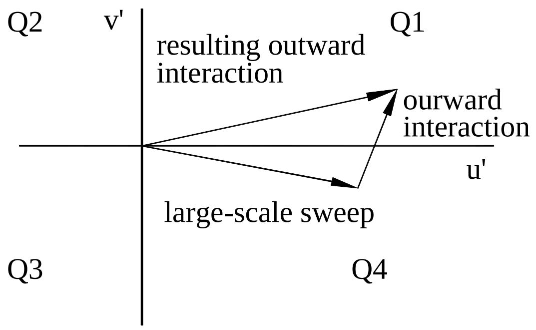

Figure 6.1: Illustration of a combination of a sweep and an outward interaction creates an outward interaction.

steady force. The lift force caused by small-scale structures such as vortices seem to be important for the initiate the motion of the stone. The vortex gives the stone a first lift then a following fluid package with increased u-velocity move the stone further over its pivot point.

From section **??** it can be seen that the forces acting on the stone might be long enough in order to dislodge the stone. In Figure 5.2, the (instantaneous) values of force-indicators of some events are quite high but the stone did not pivot, just rocked. However, when averaging these values over a certain period of time (as depicted in Figure 5.3, they become less intense and we get more pronounced distinction of the extreme values. In this experiment, the duration of 0.201s (3 frames before and 1 frame after movement) is found to give significant forces in dislodging the stone. This duration can be determined more accurately if higher sample rate is chosen to make the recordings. However, in principle this duration can be different for quasi-steady forces and TWP forces. The TWP forces are considered to give the first lift so they seem not to be last long while quasi-steady forces should be long enough. This is supported by the fact that when averaging, the quasi-steady force-indicator values decreased more drastically than the TWP force-indicator values.

6.2 Conclusions

The result derived from the B009 data is a supplement to previous information by Hofland and Booij (2004). The results of the experiment are not sufficient to draw a strong conclusion because in this experiment, there are only 4 moving events (entrainments), not very much for inspecting conditionally averaged and instantaneous flow fields. However, some conclusions can be derived here. These conclusions apply to a single stone with its specific position, shape, size, and density but can be illustrative for the entrainment process of coarse bed material.

The stone usually entrains during the time in which the horizontal velocity near the bed increases. The stone often gets an initial lift by fluctuating vertical velocity which makes the stone be more exposed to the flow. Then, the following increased u-velocity fluid package reaching the stone moves it further. The causes of the initial lift can be small-scale structures such as a vortex, an *outward interaction* (this experiment) or an *ejection* (previous experiments).

In this experiment, the increased longitudinal velocity is also part of a large-scale sweep motion as discerned in uniform flow by Hofland and Booij (2004). This is the cause of quasi-steady forces on the stone.

The results from the data B009 also support a previous conclusion by Hofland and Booij (2004) that the fluctuating vertical velocity is caused by single vortices (even #75, 175) or vortex packets (even #125) close to the stone (the size of the vortex approximately $0.5 - 2d$) which cause turbulence wall pressure fluctuations.

Besides the values, the duration in which the forces act on the stone is also important in dislodging the stone. A high values of forces but last only very short time may not sufficient to move the stone.

Acknowledgements

I would like to express my thanks to Bas Hofland and Rohnen De Ruijter, the owners of these experiments, for their guidance, enthusiasm, valuable advice and assistance with so much warmth. I also thank my promoter/supervisor Professor Marcel J.F. Stive and ir. Henk Jan Verhagen for their guidance and encouragement. I owe a special thanks to my roommate, Mohamed Fathy Mohamed Yossef, for his help and advice during writing this report.

List of Symbols

Roman symbols

$< u >_A$	velocity averaged over area A
a	proportional coefficient
A_D	exposed surface area in y-z plane
A_L	exposed surface area in x-z plane
b	proportional coefficient
B	flume width
BFS	back-ward facing step
C	smoothness coeffiction
C_D	drag coeffiction
C_{dxf}	drag coeffiction found by Xingkui & Fontijn
C_L	lift coeffiction
d	grain (stone) diameter
d_n	nominal diameter
d_{n50}	mean nominal diameter
F_1	friction force
F_2	resistance force
F_A	QSF force indicator averaged over area A
F_D	drag force
F_L	lift force
Fr	Froude number
g	gravitational acceleration
h	water depth
H	the height of the BFS
k_r	equivalent roughness
p'	pressure fluctuation
QSF	quasi-steady force
Re	Reynolds number
Re_*	particle Reynolds number $= \frac{u_* d_{n50}}{\nu}$
t	time
TWP	turbulence wall pressure
u	velocity in streamwise direction
U	mean bulk velocity
u'	fluctuation part of u

u_*	shear velocity
$u_{0.15}$	velocity measured at 0.15d above the top of the grain
U_1	mean bulk velocity at upstream of BFS
U_2	mean bulk velocity at 500 cm downstream of BFS
U_{bulk}	mean bulk velocity
$\overline{u}$	time-averaged velocity
v	velocity in vertical direction
V	volume of the grain (stone)
v'	fluctuation part of v
x	coordinate in streamwise direction
y	coordinate in vertical direction
z	coordinate in transverse direction

Greek symbols

ν	kinematic viscosity
Ψ	mobility (Shields) parameter
Ψ_c	critical Shields parameter
ρ_s	density of stone
ρ	density of water
$\sigma(v)_B$	spatial standard deviation of v in area B near the target stone

List of Figures

2.1 Forces acting on particles resting on the bed surface 4

3.1 Overview of locations of measuring areas 8
3.2 Side view of the BFS 9
3.3 The distributions of mean and standard deviation of longitudinal velocity. 10
3.4 PIV set-up 11

4.1 Procedures of data processing. 13

5.1 Areas used for averaging. The target stone is located at (x,y)=(0,0). . . . 17
5.2 Classification of events (instantaneous). 17
5.3 Classification of events (averaging). 18
5.4 Force-indicator for event #75. 19
5.5 Force-indicator for event #125. 20
5.6 Sequence of conditionally averaged flow fields (contour). 21
5.7 Sequence of conditionally averaged flow fields (vector). 22
5.8 Sequence of conditionally averaged flow fields of both entrainment and rocking events. 24
5.9 Large-scale spliced and conditionally averaged recording for sweep events. 25
5.10 Detail of typical instantaneous flow field with single vortex before movement of the target stone. 26
5.11 Detail of typical instantaneous flow field with small hairpin vortex packet before movement of the target stone. 26
5.12 The instantaneous flow field just before the entrainment. 27
5.13 Large-scale spliced flow field of sweep event # 75. 28
5.14 Large-scale spliced flow field of TWP event #125 29

6.1 Illustration of a combination of a sweep and an outward interaction creates an outward interaction. 31

References

Adrian, R. J., Christensen, K. T., Liu, Z.-C. (2000, Spring). Analysis and interpretation of instantaneous turbulent velocity fields. *Experiments in Fluids*, *29*, 275-290.

Booij, R., Hofland, B. (2004). Measurement of the mechanisms of stone entrainment. *River flow*, *1*, 821-830.

Chien, N., Wan, Z. (1998). *Mechanics of sediment transport.* ASCE Press. (English Translation)

De Ruijter, R. (2004). *Turbulence structures affecting stone stability in backward-facing step flow (subtitle: Experiments by means of particle image velocimetry).* M.sc thesis, Delft University of Technology.

Hofland, B. (2002). Near-bed turbulence and stone stability theory and measurements. *Draft.*

Hofland, B. (2003). Measurement of fluctuating pressures on coarse bed material. *Journal of Hydraulic Engineering.* (Submitted)

Hofland, B., Booij, R. (2004). Measuring the flow structures that initiate stone movement. *River flow, 1.*

Schiereck, G. (2001). *Introduction to bed, bank and shore protection.* Delft, The Netherlands: Delft University Press.

Xingkui, W., Fontijn, H. L. (1993). Experimental study of the hydrodynamic forces on a bed element in an open channel with a backward-facing step. *Journal of Fluids and Structures*, *7*(3), 299-318. (TY - JOUR)